

Simulations of Biomass Burning Plumes using a Three-Dimensional Transport Model and Comparisons of Simulated Optical Properties to *In Situ* and Remote Sensing Observations

Authors: R. I. Matichuk¹, P. R. Colarco² and O. B. Toon¹

¹Laboratory for Atmospheric and Space Physics, Program in Atmospheric and Oceanic Sciences, University of Colorado, Boulder, CO, 80309

²Earth System Science Interdisciplinary Center, University of Maryland-College Park, NASA Goddard Space Flight Center, Code 916, Greenbelt, MD, 20771

Abstract. In this study, we model the evolution of biomass burning aerosols and investigate its optical properties. Our model is driven by assimilated meteorology from the NCEP/NCAR reanalyses and constrained with measurements collected during the Southern African Aerosol Regional Science Initiative campaign (SAFARI 2000). To model the smoke aerosols properly, detailed simulations were conducted to determine the effects of various aerosol transport processes (smoke injection height and diurnal cycle) and aerosol microphysical processes (coagulation and evolving aerosol size distributions). Modeled smoke aerosol optical thickness, aerosol extinction, and angstrom exponent were compared to satellite, aircraft and ground-based observations made over central and southern Africa. The modeled aerosol distributions were found to be sensitive to injection heights greater than 3 km, and the aerosol optical properties were found to be sensitive to the treatment of coagulation and the evolution of a particle size distribution. The transport of smoke was found to be insensitive to the implementation of a diurnal cycle on emissions. In addition, the model aerosol optical properties were comparable to observations at locations and times where smoke plumes were present. However, our model under-estimated or over-estimated the optical properties by up to a factor of two. Air mass back-trajectories at various locations were also conducted to compare with our model results. The trajectories suggest that it is possible for the smoke aerosols to be present at the locations where our model is identifying smoke plumes, but also that other aerosol species are likely to contribute to the observed aerosol optical properties. These results will be useful in future applications relating to the transport and evolution of smoke aerosols from biomass burning fires.

Introduction

Biomass burning has a large regional and global impact on the distribution of trace gases and aerosols in the atmosphere [Crutzen and Andreae, 1990; Hobbs et al., 1997; Scholes et al., 1996; Hao et al., 1990]. The aerosols that come from both natural and anthropogenic burning of vegetation have a significant impact on the carbon cycling in ecosystems, air quality, and the atmospheric chemistry and radiation budget. It is believed that a significant source of aerosols and trace gases is produced from the burning of natural vegetation in central and southern Africa [Hao et al., 1990; Andreae, 1991]. Studies have shown that the savannas of Africa experience the most extensive biomass burning in the world, thereby being the largest source of aerosol black carbon (BC) [Dwyer et al., 1998; Holben et al., 2001].

Biomass burning impacts our air quality by degrading the visibility. Smoke aerosols have been observed to degrade visibility both locally and regionally. Studies have observed smoke plumes being transported far distances away from smoke sources [Posfai et al., 2003, Colarco et al., 2004]. Figure 1 is a satellite image of smoke aerosols being transported across southern Africa and over the Indian Ocean on September 4, 2000 [SeaWiFS Project, NASA/Goddard Space Flight Center, and ORBIMAGE].

Biomass burning also impacts the atmospheric chemistry and radiation budget. These fires produce large amounts of aerosol and trace gas species (CO and NO_x) that are important precursors to photochemical production of tropospheric ozone [Goode et al., 2000]. In addition, studies have estimated that the global mean surface forcing due to smoke aerosols to be -0.2 Wm⁻² with an

uncertainty as large as a factor of 3 and a 'very low' level of scientific understanding (Figure 2) [IPCC, 2001]. In order to reduce this uncertainty, more research on the transport, evolution and radiative effects of the biomass aerosols needs to be completed.

Project Description

In this study, we simulated the transport and evolution of biomass burning plumes using a three-dimensional transport model and compared the model optical properties to *in situ* and remote sensing observations. In order to model the smoke aerosols properly, detailed simulations were conducted to determine (1) how the transport of smoke aerosols was sensitive to aerosol emissions and (2) how the model optical properties were sensitive to the evolution of a particle size distribution. Four sensitivity tests were conducted to test the model's sensitivity to aerosol emissions and evolving a particle size distribution.

Sensitivity Test #1: This test investigates the altitude at which the smoke aerosols are being injected into the atmosphere. Observations show that aerosols produced from fires are being injected into the atmosphere at various altitudes [Colarco et al., 2004; Schmid et al., 2003; Haywood et al., 2003; McGill et al., 2003]. Here the observations show smoke aerosols being emitted from the surface to 5 km above ground level (AGL). The injection height of aerosol emissions from biomass burning are assumed to be associated with a lift due to the release of thermal heat in the fires, which is mainly dependent on the type of vegetation being burned and combustion type (smoldering or flaming) [Stock et al. 1996; Andreae and Merlet et al., 2001].

Four cases were conducted for this test, each case using different methods of emitting aerosols into the model. Figure 3 shows a schematic of the four cases and where the aerosols were emitted into the model for each case. In one case, aerosol emissions were evenly distributed between 1 km and 4 km. In

another case, the aerosol emissions were evenly distributed from the planetary boundary layer height (PBLH) to the layer above. In the third case, the aerosol emissions were evenly distributed from the surface to the PBLH. And in the final case, the aerosol emissions were only emitted at the surface of the model. These conditions were based on spaceborne, airborne and ground-based observations and the altitude of the PBLH was based on the measurements from MATCH and assimilated meteorology from NCEP/NCAR reanalyses.

Sensitivity Test #2: This test investigated a diurnal cycle on emissions. A study by Eck et al., 2003 observed a significant average diurnal trend over six sites in Zambia with a minimum AOT₅₀₀ at 0900 UTC and maximum at 1500 UTC. This diurnal cycle in aerosol loading is possibly caused by a diurnal cycle in the number of biomass burning fires and their intensity. Higher air temperatures, lower relative humidity, and higher wind speeds at midday and afternoon may result in more intense and faster moving fires at those times of the day. In addition, agricultural practices take advantage of these favorable conditions and start more fires in the late morning.

Two cases were conducted for this test. In one case, aerosol emissions were evenly distributed over a 12-hour period in the model (between the '06' hour to the '18' hour time-steps). In the second case, the aerosol emissions were consistently distributed over a 24-hour period in the model. The time periods at which aerosol were emitted in the model are in agreement with observations by Eck et al. [2003].

Sensitivity Test #3: This test observes the effects of coagulation on the model optical properties. Coagulation is the merging of aerosols into a single, larger aerosol thereby decreasing the number of aerosols but not changing the volume concentration. The size of the aerosol is important when calculating

its optical properties because different size particles scatter different amounts of radiation.

Two cases were conducted for this test. In one case, the aerosols were allowed to coagulate (i.e. coagulation process was turned ‘on’). And in the other case, the aerosols were not allowed to coagulate (i.e. coagulation process was turned ‘off’). In the model, the aerosols coagulated via Brownian coagulation.

Sensitivity Test #4: This test observes the effects of employing a ‘fresh’ smoke particle size distribution. A ‘fresh’ smoke particle size distribution is a distribution that is representative of smoke aerosols that are less than a few minutes old [Haywood et al., 2003]. Two cases were conducted for this test, each case using a different initial particle size distribution. In one case, the model was initialized with a fresh particle size distribution measured by a PCASP instrument over Otavi, Namibia, Africa on September 13, 2000 [Haywood et al., 2003]. In the other case, the model was initialized with a fresh particle size distribution retrieved by an AERONET instrument over Ndola, Zambia, Africa on September 16, 2000. Figure 4 shows the two particle size distributions.

All of the sensitivity test simulations were initialized with a ‘base case’ and ran for a duration of two months. The base case had no transformation processes active (i.e. no coagulation), aerosol emissions were emitted between the surface and PBLH, only smoke aerosols were transported throughout the model (i.e. no dust or sea salt aerosols), and the model transported a ‘fresh’ particle size distribution observed by a PCASP instrument over Otavi, Namibia, Africa on September 13, 2000 [Haywood et al., 2003].

Optical Property Calculations

Aerosol optical thickness (AOT), aerosol extinction, and the angstrom exponent (α) were calculated using Mie Theory and assuming a refractive index representative of

fresh smoke aerosols ($RI = 1.54 - 0.018i$) [Haywood et al., 2003]. AOT is the attenuation of radiant energy through a column of air (Equation 1). Aerosol extinction is the attenuation of radiant energy through a specific layer within a column of air (Equation 2). And, α is the slope of the AOT versus the difference in a wavelength pair (Equation 3). The angstrom exponent is commonly used to characterize the wavelength dependence of AOT of a particular wavelength pair and provides basic information on the aerosol size distribution. In general, a small value of α ($\alpha < 1$, relatively little dependence of AOT on wavelength) is associated with large particles (i.e. dust and sea salt particles) while larger values of α are associated with small particles (i.e. smoke particles).

Equation 1:

$$AOT = \tau = \int_0^{\infty} \int_0^{\infty} \pi r^2 N(r, z) q_{ext} dr dz$$

where N is the size distribution ($\# \text{ cm}^{-3} \mu\text{m}^{-1}$), q_{ext} is the extinction efficiency.

Equation 2:

$$Aerosol \text{ Extinction} = \int_{x_1}^{x_2} \int_0^{\infty} \pi r^2 N(r, z) q_{ext} dr dz$$

where N is the size distribution ($\# \text{ cm}^{-3} \mu\text{m}^{-1}$), q_{ext} is the extinction efficiency.

$$Equation \ 3: \quad \alpha = - \frac{\ln\left(\frac{\tau_{a_2}}{\tau_{a_1}}\right)}{\ln\left(\frac{\lambda_2}{\lambda_1}\right)}$$

where λ_1 and λ_2 are a pair of measurement wavelengths τ_{a1} and τ_{a2} are the AOT values measured at those wavelengths.

Comparison to Datasets

The model optical properties were compared to satellite, aircraft and ground-based observations made over central and southern Africa. For this study, the model results were only compared at two locations

in southern Africa; Etosha Pan, Namibia, Africa and Inhaca, Mozambique, Africa (Figure 5). These locations were selected based on their proximity to aerosol emissions. My interest was to compare a location with fresh smoke aerosols or a location near an aerosol source (Inhaca) to a location with aged smoke aerosols (i.e. aerosols that were more than an hour old) or a location far from an aerosol source (Etosha Pan).

Spaceborne Measurements:

Total Ozone Mapping Spectrometer (EP-TOMS)

EP-TOMS is onboard the Earth Probe satellite and makes radiation measurements at two near-UV channels to calculate aerosol optical depth and single scattering albedo [Torres et al., 1998]. The retrieval technique applied to the EP-TOMS data makes use of two advantages of near-UV remote sensing not available in the visible or near IR; the low reflectivity of all land surface types and the high sensitivity to aerosol types that absorb in the UV, allowing clear separation between carbonaceous and mineral aerosols (smoke aerosols) from purely scattering aerosols (sulfates and sea salt aerosols). A drawback in using EP-TOMS data is that it cannot observe aerosols below 2 km.

Moderate Resolution Imaging Spectroradiometer (MODIS)

MODIS is onboard the Earth Observing System's (EOS) Terra satellite and makes retrievals at seven spectral bands to calculate aerosol optical thickness over the ocean and land [Kaufman et al., 1997]. The disadvantage of MODIS is that it has problems making retrievals over bright surfaces; thus retrievals cannot be made over deserts and snow.

Along Track Scanning Radiometer (ATSR)

ATSR is onboard the European ERS-2 satellite, which was launched in April 1995, and provides daily global maps showing locations of hot spots [Arino et al., 1995].

ATSR has four visible and infrared channels centered at 550 nm, 670 nm, 870 nm and 1600 nm and three thermal infrared channels centered at 3700 nm, 11000 nm and 12000 nm. The spatial resolution is approximately 1 x 1 km² at nadir. The swath of 512 km allows a revisiting period of 3 days at the equator and the satellite cycle is 35 days. The ATSR has a conical scanning mechanism that produces two views of each region; a forward view (zenith angle approximately 55 degrees) and about two minutes later a nadir view.

Airborne Measurements:

NASA Ames Airborne Tracking 14-Channel Sun Photometer (AATS-14)

The AATS-14 measures the transmission of the direct solar beam in 14 spectral channels (354 nm to 1557 nm) [Schmid et al. 2003]. During the SAFARI 2000 campaign, measurements were made over seven locations in southern Africa.

Ground-Based Measurements:

Aerosol Robotic Network (AERONET)

AERONET is a globally dispersed network of automatic ground-based Sun/sky scanning radiometers from which aerosol optical thickness, cloud water vapor, aerosol particle size distributions and aerosol single-scattering albedo are retrieved [Holben et al., 1998]. Seventeen southern Africa AERONET sites were operational during the SAFARI 2000 campaign (Figure 5).

Back Air Mass Trajectories

Kinematic back trajectories were run with the NASA/GSFC trajectory model [Schoebel and Sparling, 1995]. NCEP/NCAR reanalyses were used to drive the calculations [Kalnay et al., 1996]. For this study, several back trajectories were performed in order to identify where and at what altitudes the aerosols were coming from during September 2000. The back trajectories went back five days and were initialized at six altitudes (1 km, 3 km, 5 km, 7 km, 9 km, 11 km) over various locations in southern Africa.

Model Description

A three-dimensional aerosol and microphysical transport model was used to simulate the transport and evolution of smoke aerosols from biomass burning fires. The Community Aerosol and Radiation Model for Atmospheres (CARMA) has been developed at NASA Ames Research Center and the University of Colorado. The three-dimensional implementation of this model is documented in Toon *et al.* [1998]. The current version of the model uses a bin representation of the aerosol particle size distribution and is capable of treating multiple aerosol types simultaneously so that mixtures and multi-component aerosols can be included. The model also includes all basic microphysical processes affecting aerosols and clouds. These processes include nucleation, condensational growth and evaporation, coagulation, sedimentation, advection by winds, dry deposition, wet removal, and surface fluxes for constituent input. Transport and aerosol growth are solved using a numerically accurate, highly non-diffusive piecewise polynomial algorithm following Lin and Rood [1996]. In addition, this model can simulate any date that is available in the global wind archives and can expand or contract its grid to encompass any location on the Earth. CARMA is driven by meteorological fields derived from the NCAR Model for Atmospheric Transport and Chemistry (MATCH) [Rasch *et al.*, 1997]. MATCH is an offline version of the NCAR Community Climate Model (CCM), driven by NCEP/NCAR reanalyses assimilated meteorology and contains the same basic physics parameterizations that are included in CCM version 3. MATCH is a global model that is run at the resolution of the input meteorology (typically $1.875^\circ \times 1.875^\circ$ in the horizontal and 28 levels in the vertical for the NCEP/NCAR reanalyses). CARMA runs on the same $1.875^\circ \times 1.875^\circ$ grid as MATCH. A

30-day spin-up time is needed in order to input enough aerosols into the model.

This model has been previously applied to three-dimensional simulations of the transport and evolution of carbonaceous aerosols produced by biomass burning, mineral dust, and sea salt aerosols. The simulated aerosol results are documented in Westphal and Toon [1991a,b] and Colarco *et al.* [2002, 2003a,b, 2004].

To constrain our model, we used various observations and measurements obtained from the Southern African Regional Science Initiative (SAFARI 2000) [Swap *et al.*; 2003]. SAFARI 2000 investigated the emissions, transport, transformation and deposition of trace gases and aerosols during the dry and wet seasons over southern Africa during 1999-2000. Figure 6 shows the distributions of fires observed by ATSR during the month of September 2000 over central and southern Africa. The majority of the fires observed during the SAFARI 2000 campaign was of anthropogenic origin and were prescribed in the early part of the dry season as a land management tool. The burning of wetter soils at the beginning of the dry season produced lower fire intensities, which resulted in less vegetation consumed and damage to the soil. Pastoralists burned extensively in the early dry season for rapid nutrient release prior to the new growing season by farmers and to stimulate regrowth of palatable grasses for their cattle. Early burning was also used in national parks as a preventative measure against late dry season fires, which tended to have higher intensities and be presumably be more destructive. Fires were also used to maintain the competitive balance between trees and grasses. The vegetation cover over most of central and southern Africa included evergreen forests, arid/moist woodlands, savannas and wooded grasslands (Figure 6) [Scholes *et al.*, 1996]. The aerosols produced from these fires were carbonaceous-based particles and total average carbon emitted per year from these fires ranged from 205 to 785 Tg yr⁻¹ (Table 1) [Scholes *et al.*, 1996;

Barbosa et al., 1999; VanderWerf et al., 2003]. SPOT-Vegetation observations estimated mean burned area of 7.83 km², maximum burned area of 1458 km², and total burned area of 95,962 km² over Africa during the SAFARI 2000 campaign [Hely et al., 2003].

Model emissions were interpolated from the Global Fire Emissions Database (GFED) [Van Der Werf et al., 2003]. This database provides 1° x 1° gridded mean monthly carbon emissions from January 1997 to December 2002. These emissions are constructed by relating TRMM-VIRS hot spot data to MODIS burned area product. In order to convert the carbon emissions to aerosol emissions, which are needed for the model, we assumed an emission factor of 5.4 g PM_{2.5} / kg of Dry Mass, which is representative of savanna and grassland vegetation and assumed that 45% of the dry mass burned was carbon [Andreae and Merlet, 2001]. Figure 5 shows the interpolated aerosol emissions that were evenly distributed in the model over the month of September 2000.

Results

Model results:

Sensitivity Test # 1:

Figure 7 shows the monthly mean vertical profile of aerosol mass concentrations at various altitudes for each case during the month of September 2000. These results show that the vertical transport of aerosols is only sensitive to when the aerosols are emitting between 1 km and 4 km at a location is near an emission source (left figure). However, at a location far from an emission source (Etosha Pan), the transport of aerosols is insensitive to the altitudes at which the aerosols are emitted (right figure).

Sensitivity Test #2:

Figure 8 shows the daily mean AOT at 500 nm (AOT₅₀₀) for the month of September 2000 over Inhaca (left figure) and Etosha Pan (right figure). These results show that the transport of aerosols in our model is

insensitive to the implementation of a diurnal cycle on emissions.

Sensitivity Test #3:

Figure 9 shows the daily mean normalized volume aerosol size distribution on the first and last day of the simulation over Inhaca. Here the results show that coagulation changes the volume aerosol size distribution by producing higher concentrations of larger aerosols.

Figure 10 shows the daily mean AOT₅₀₀ for the month of September 2000 over Inhaca (left figure) and Etosha Pan (right figure). These results show that the simulated aerosol optical properties are sensitive to coagulation.

Sensitivity Test #4:

Figure 11 shows the daily mean AOT₅₀₀ for the month of September 2000 over Inhaca (left figure) and Etosha Pan (right figure). Here results show that the initialization with various size distributions does not affect the simulated aerosol optical properties.

Model Results Compared to Datasets:

Comparison to EP-TOMS:

Figure 12 shows the modeled monthly mean AOT₅₅₀ over Africa for September 2000. Here, the model was initialized a fresh smoke aerosol size distribution observed by a PCASP measurement over Otavi, Namibia, Africa on September 13, 2000, aerosols were emitted from the surface to PBLH, and the aerosols were allowed to coagulate. Figure 13 shows the monthly mean EP-TOMS aerosol index at 360 nm for September 2000. Even though EP-TOMS figure is not presenting AOT, its results can be compared to the model results because the aerosol index is proportional to AOT when the aerosols are highly absorbing and at high altitudes. Several back air mass trajectories conducted over Etosha Pan and Inhaca suggest that smoke aerosols were being transported at high altitudes during the month of September; thereby allowing the EP-TOMS aerosol index to be proportional to the model AOT₅₅₀. The

comparison of Figure 12 to Figure 13 shows that both the model and EP-TOMS are observing the same smoke plume signature over southern Africa and over the Atlantic Ocean.

Comparison to MODIS:

Figure 14 shows MODIS monthly mean AOT₅₅₀ over Africa for September 2000. The modeled AOT₅₅₀ (Figure 12) is comparable to MODIS (Figure 14) where both results identify the same smoke plume signature over central and southern Africa and over the eastern Atlantic Ocean. However, the model results are under-estimating the aerosol optical thickness by up to a factor of 2. This may be due to the aerosol retrievals made by MODIS. Here the MODIS retrievals are measuring all aerosol particles (i.e. smoke, dust and sea salt aerosols) whereas the model is only modeling smoke aerosols.

Comparison to AATS-14:

Figure 15 shows the vertical profile of aerosol extinction at various altitudes for September 16, 2000 over Etosha Pan. The model results are only comparable to the AATS-14 measurement at altitudes below 2 km. Both results show an aerosol layer between the surface and 2 km. However, the model result is not identifying the aerosol layer above 2 km that is being observed by the AATS-14 measurement. The model may not be identifying the elevated aerosol layer because it may be a cloud. However back air mass trajectories performed on September 16, 2000 over Etosha Pan suggest that the elevated layer is an elevated aerosol layer since air masses between 2 km and 4 km originated over locations with smoke sources (Figure 16).

Comparison to AERONET:

Figures 8, 10 and 11 show AERONET and modeled daily mean AOT₅₀₀ from Sensitivity Test #2, Sensitivity Test #3, and Sensitivity Test #4, respectively. The modeled AOT₅₀₀ are comparable to

AERONET AOT₅₀₀ at locations and times where smoke plumes were present. However, the model over-estimates or under-estimates the AOT₅₀₀ by up to a factor of two.

In order to understand the aerosol size distributions, daily mean angstrom exponents were computed at three wavelength pairs (440 nm/870 nm, 380 nm/500 nm, and 500 nm/870 nm) using the results from Sensitivity Test #3 and compared to daily mean AERONET angstrom exponents on the 13 and 22 of September 2000 at Etosha Pan (Table 2). The estimated angstrom exponents are much greater than 1, which suggests that the measurements from the 13 and 22 of September 2000 over Etosha Pan were dominated by small particles. Back air mass trajectories suggest that the small smoke particles were representative of smoke aerosols since the air masses originated over locations with smoke sources (Figures 17 and 18).

These calculations also show that when coagulation was active, the angstrom exponents were similar to AERONET. However, when coagulation was not active, the angstrom exponent was much higher compared to AERONET. Thus, it is important for the aerosols to coagulate in order for the model results to be comparable to AERONET measurements. The modeled angstrom exponents from the coagulation case were however slightly higher than AERONET suggesting that our initial aerosol size distribution contains too many small particles.

Summary

Simulations show that the transport of aerosols in our model are sensitive to aerosol emissions being injected between 1 km and 4 km but insensitive to when the aerosols are emitted during the day. Simulations also show that the modeled aerosol optical properties are sensitive to the coagulation of aerosols but insensitive to the initial aerosol size distribution. Here, coagulation was found to create higher concentrations of larger aerosols after a two-month simulation.

Modeled optical properties were comparable to other datasets at locations and times where smoke plumes were present. The modeled monthly mean AOT₅₅₀ identified the same smoke signature over central and southern Africa as compared to MODIS monthly mean AOT₅₅₀ and EP-TOMS aerosol index. The modeled daily mean AOT₅₀₀ were also similar to AERONET daily mean AOT₅₀₀. However, the model results were over-estimating or under-estimating AOT by up to a factor of 2. In addition, the modeled daily mean vertical profiles were comparable to the AATS-14 measurements at altitudes below 2 km. Both results identify an aerosol layer below 2 km. However, the model is missing the aerosol layer above 2 km. The AERONET angstrom exponent suggests that we are emitting too many small aerosols into our model since the modeled angstrom exponents are slightly larger than the AERONET measurements. Lastly, back air mass trajectories suggest that it is possible for the smoke aerosols to be present at the locations where our model is identifying smoke plumes, but also that other aerosol species are likely to contribute to the observed aerosol optical properties.

Future Work

In order to explain the over-estimated and under-estimated optical properties, I plan to run two more sensitivity tests. One sensitivity test would include running the model with a different aerosol emissions dataset. For this test, I would like to run the model with a carbon emission dataset prepared by Korontzi et al. [*in press*]. Here the carbon emissions are estimated by using the most recent version of Global Burned Area product (GBA-2000), released in December 2002, MODIS percent tree cover to distinguish between ecosystems (i.e. grassland vs. savanna), and TRMM active fire data. In another sensitivity test, I would like to correlate the carbon emissions to the MODIS fire count product. Currently, the emissions are being evenly distributed over the month; however in using the MODIS

fire count product, I would like to only emit aerosols on days when MODIS is identifying a fire. Lastly, I would like to compare the modeled optical properties to MODIS daily AOT₅₅₀ for fine particles.

References

Andreae, MO & P Merlet, Emission of trace gases and aerosols from biomass burning, *Glob. Biogeo. Cycles*, 15 (4), 943, 2001.

Arino, O, A Buongiorno, P Goryl, Intercalibration of AVHRR and ATSR data, Calibration and Applications of Satellite Sensors for Environmental Monitoring *Advances in Space Research*, 17 (1)29-38 1995.

Barbosa PM, Stroppiana D, Gregoire JM, Pereira JMC, An assessment of vegetation fire in Africa (1981-1991): Burned areas, burned biomass, and atmospheric emissions, *Global Biogeochemical Cycles*, 13 (4): 933-950, DEC 1999

Colarco, PR, OB Toon, O Torres & PJ Rasch, Determining the UV imaginary index of refraction of Saharan dust particles from TOMS data and a three dimensional model of dust transport, *J. Geophys. Res.*, 107, 4289, 2002.

Colarco, PR, OB Toon & B Holben, Saharan Dust Transport to the Caribbean during PRIDE: 1. Influence of dust sources and removal mechanisms on the timing and magnitude of downwind AOD events from simulations of in situ and remote sensing observations, *J. Geophys. Res.*, 108 (D19), 8589, 2003.

Colarco, PR, OB Toon, JS Reid, JM Livingston, PB Russell, J Redemann, B Schmid, HB Maring, D Savoie, EJ Welton, JR Campbell, BN Holben & R Levy, Saharan Dust Transport to the Caribbean during PRIDE: 2. Transport, vertical profiles, and deposition in simulations of in situ and remote

- sensing observations, *J. Geophys. Res.*, 108 (D19), 8590, 2003.
- Colarco, PR, MR, Schoeberl, BG Doddridge, LT Marufu, O Torres, & EJ Welton, Transport of smoke from Canadian forest fires to the surface near Washington, D. C.: Entrainment and optical properties, in press, *J. Geophys. Res.*, 2004.
- Crutzen, OJ, Andreae, MO, Biomass burning in the tropics – Impact on atmospheric chemistry and biogeochemical cycles, *Science*, 250, 4988: 1669-1678, Dec. 21, 1990.
- Dwyer, E, JM Pereira, JM Gregorie, and CC DaCamara, Characterization of the spatio-temporal patterns of global fire activity using satellite imagery for the period April 1992 to March 1993, *J. of Biogeography*, 27(1), 57-69, 2000.
- Dwyer, E, JM Gregoire, and JP Malingreau, A global analysis of vegetation fires using satellite images: Spatial and temporal dynamics, *Ambio*, 27, 175-181, 1998.
- Goode, JG, RJ Yokelson, DE Ward, RA Susott, RE Babbitt, MA Davies, & WM Hao, Measurements of excess O₃, CO₂, CO, CH₄, C₂H₄, C₂H₂, HCN, NO, NH₃, HCOOH, CH₃COOH, HCHO, and CH₃OH in 1997 Alaskan biomass burning plumes by airborne Fourier transform infrared spectroscopy (AFTIR), *J. Geophys. Res.*, 105, 2147-2166, 2000.
- Eck TF, BN Holben, DE Ward, MM Mukelabai, O Dubovik, A Smirnov, JS Schafer, NC Hsu, SJ Piketh, A Queface, JL Roux, RJ Swap and I Slutsker, Variability of biomass burning aerosol optical characteristics in southern Africa during the SAFARI 2000 dry season campaign and a comparison of single scattering albedo estimates from radiometric measurements, *J. Geophys. Res.*, 108 (D13), 8477, 2003
- Hao, WM, MH Liu, PJ, Crutzen, Estimates of annual and regional releases of CO₂ and their trace gases to the atmosphere from fires in the tropics, based on the FAO statistics for the period 1975-1980, *Fire in the Tropical Biota: Ecosystem Processes and Global Challenges*, *Ecol. Studies* 84 (ed. Goldammer), pp. 440-462. Springer-Verlag, New York, 1996.
- Haywood, J, SR Osborne, PN Francis, A Keil, P Formenti, MO Andreae, and PH Kaye, The mean physical and optical properties of regional haze dominated by biomass burning aerosol measured from C-130 aircraft during SAFARI 2000, *J. Geophys. Res.*, 108 (D13), 8473, 2003
- Hely C, Caylor K, Alleaume S, RJ Swap, HH Shugart, Release of gaseous and particulate carbonaceous compounds from biomass burning during the SAFARI 2000 dry season field campaign, *J. Geophys. Res.*, 108 (D13): Art. No. 8470 FEB 13 2003
- Hobbs, PV, JS Reid, RA Kotchenruther, RJ Ferek & R Weiss, Direct Radiative Forcing by Smoke from Biomass Burning, *Science*, 275, 5307, 1997.
- Holben, BN et al., An emerging ground based aerosol climatology: Aerosol optical depth from AERONET, *J. Geophys. Res.*, 106, 12,067-12,097, 2001.
- Holben, BN et al., AERONET-A federated instrument network and data archive for aerosol characterization, *Remote Sens. Environ.*, 66, 1-16, 1998.
- Kalnay, E et al., The NCEP/NCAR 40-year reanalysis project, *Bull. Am. Meteorol. Soc.*, 77, 437-471, 1996.
- Kaufman, YJ, PV Hobbs, VWJH Kirchhoff, P Artaxo, LA Remer, BN Holben, MD King, DE Ward, EM Prins, KM Longo, LF Mattos, CA Nobre, JD Spinhrne, Q Ji, AM Thompson, JF Gleason, SA Christopher & SC

- Tsay, Smoke, Clouds, and Radiation – Brazil (SCAR-B) experiment, *J. Geophys. Res.*, 103 (D24), 31783, 1998.
- Korontzi, S, DP Roy, CO Justice & DE Ward, Modeling and sensitivity analysis of fire emissions in southern Africa during SAFARI 2000, *Remote Sens. Environ.*, in press.
- Lin, SJ and RB Rood, Multidimensional flux-form semi-Lagrangian transport schemes, *Mon. Wea. Rev.*, 124, 2046, 1996.
- McGill, Matthew J.; Hlavka, Dennis L.; Hart, William D.; Welton, Ellsworth J.; Campbell, James R., Airborne lidar measurements of aerosol optical properties during SAFARI-2000, *J. Geophys. Res.*, 108 (D13), 10.1029/2002JD002370, April 2003.
- Posfai, M, R Simonics, J Li, PV Hobbs & PR Buseck, Individual aerosol aerosols from biomass burning in southern Africa: 1. Compositions and size distributions of carbonaceous aerosols, *J. Geophys. Res.*, 108 (D13), 8483, doi: 10.1029/2002JD002291, 2003.
- Rasch, PJ, NM Mahowald & BE Eaton, Representations of transport, convection, and the hydrologic cycle in chemical transport models: Implications for the modeling of short-lived and soluble species, *J. Geophys. Res.*, 102 (D23), 28 127, 1997.
- Schmid, B, J Redemann, PB Russell, PV Hobbs, DL Hlavka, MJ McGill, BN Holben, EJ Welton, JR Campbell, O Torres, RA Kahn, DJ Diner, MC Helmlinger, DA Chu, C Robles-Gonzalez, G de Leeuw, Coordinated airborne, spaceborne, and ground-based measurements of massive thick aerosol layers during the dry season in southern Africa, *J. Geophys. Res.*, 108 (D13), 2003.
- Schoeberl, M.R. and L.C. Sparling, Trajectory modeling, in *Diagnostic Tools in Atmospheric Physics: Enrico Fermi Course CXVI*, edited by G. Fiocco and G. Visconti, pp. 289-305, North-Holland, New York, 1995.
- Scholes, RJ, J Kendall, CO Justice, The quantity of biomass burned in southern Africa, *J. Geophys. Res.*, 101, 23667-23676, 1996.
- Scholes, M and MO Andreae, Biogenic and pyrogenic emissions from Africa and their impact on the global atmosphere, *Ambio*, 29, 23-29, 2000.
- Swap, RJ, Annegarn HJ, Otter L, Southern African Regional Science Initiative (SAFARI 2000): summary of science plan, *South African Journal of Science*, 98, (3-4): 119-124, MAR-APR 2002.
- Toon, O, BR Turco, D Westphal, R Malone & M. Liu, A multidimensional model for aerosols: Description of computational analogs, *J. Atmo. Sci.*, 45, 2123, 1998.
- Torres, O, PK Bhartia, JR Herman & Z Ahmad, Derivation of aerosol properties from satellite measurements of backscattered ultraviolet radiation. Theoretical Basis, *J. Geophys. Res.*, 103, 17099-17110, 1998.
- VanDerWerf, GR, JT Randerson, J Collatz & L Giglios, Carbon emissions from fires in tropical and subtropical ecosystems, *Global Change Biology*, 9 (4), 547, 2003.
- Westphal, D, OB Toon, Simulations of microphysical, radiative, and dynamical processes in a continental-scale forest fire smoke plume, *J. Geophys. Res.*, 96, 22 379, 1991a. Westphal, D., O. B. Toon, The short-term temperature response to smoke from oil fires, *Geophys. Res. Letters*, 18, 1873, 1991b

Figures

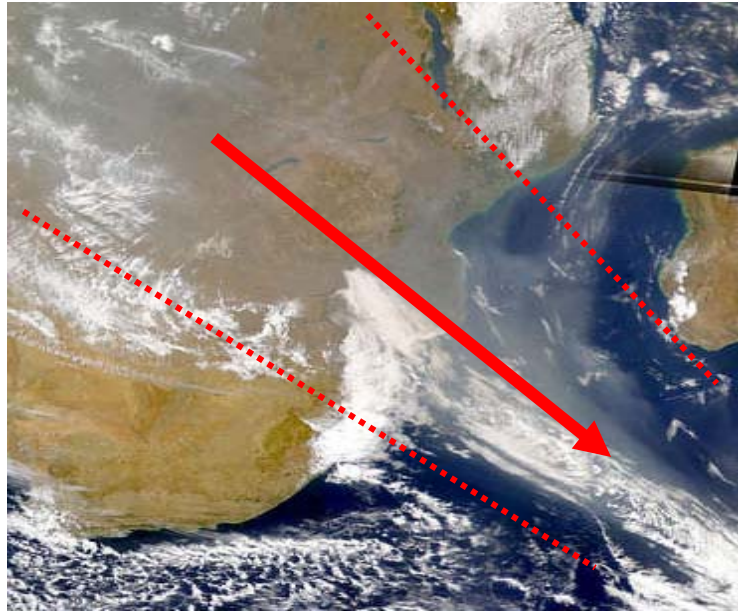


Figure 1. Central African biomass burning smoke and haze exiting off the east coast on September 4, 2000. The red arrow represents the direction of transport of the smoke and haze. Provided by the SeaWiFS Project, NASA/Goddard Space Flight Center, and ORBIMAGE.

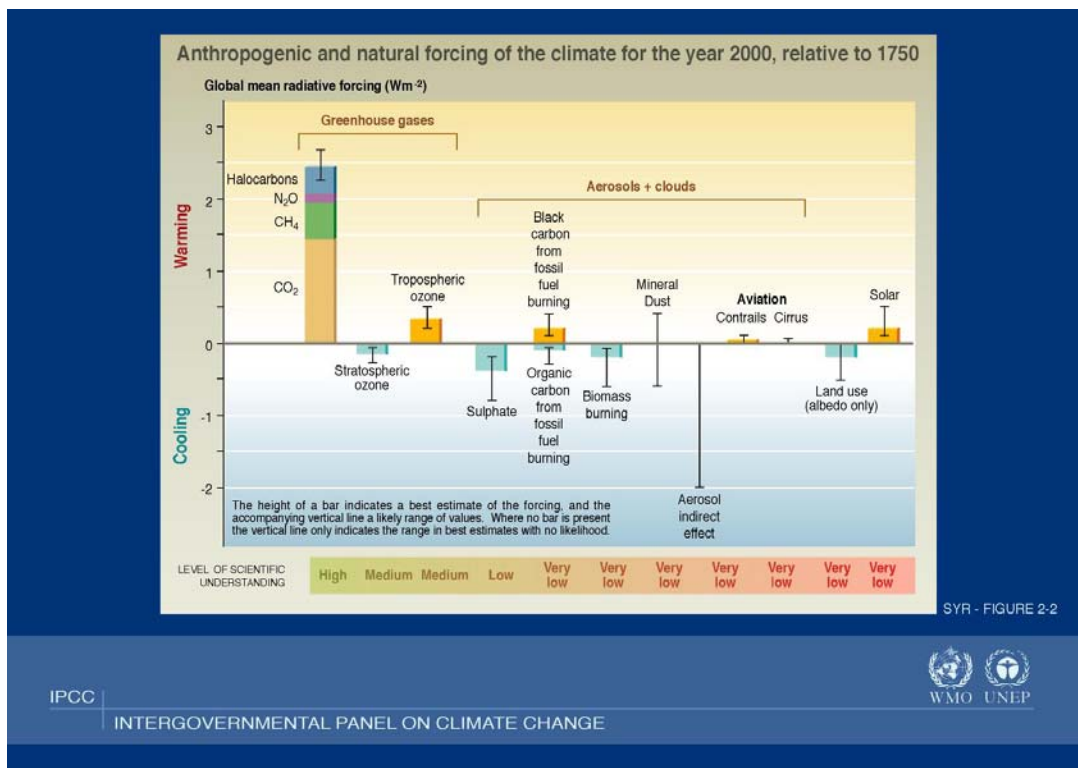


Figure 2. Anthropogenic and natural forcing of the climate for the year 2000.

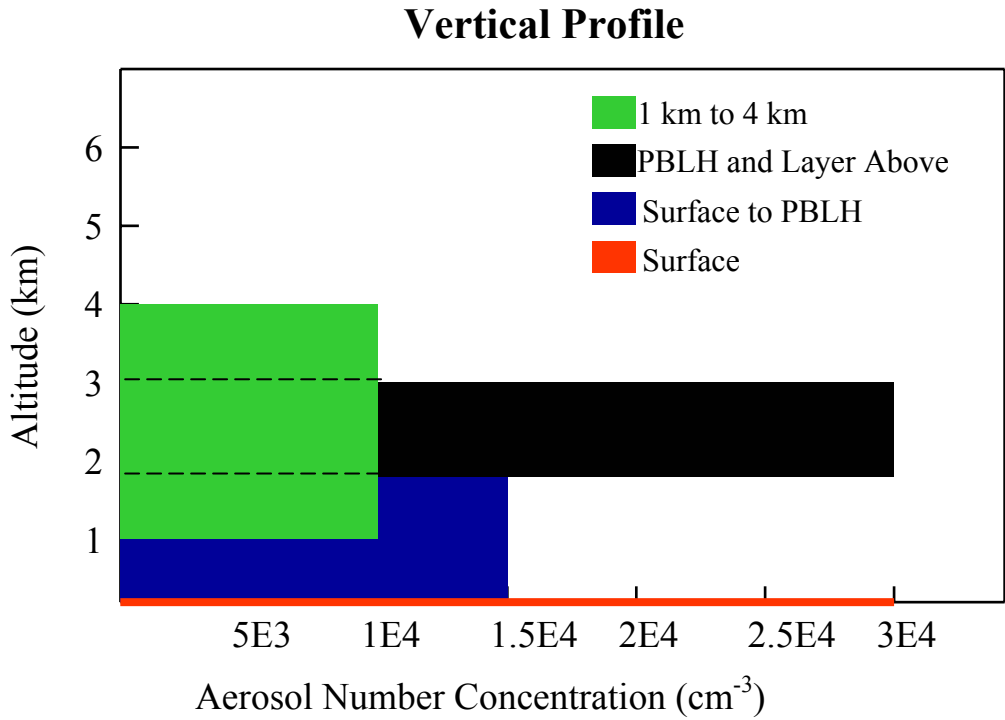


Figure 3. Shows where the aerosols were emitted into the model for each case in Sensitivity Test #1.

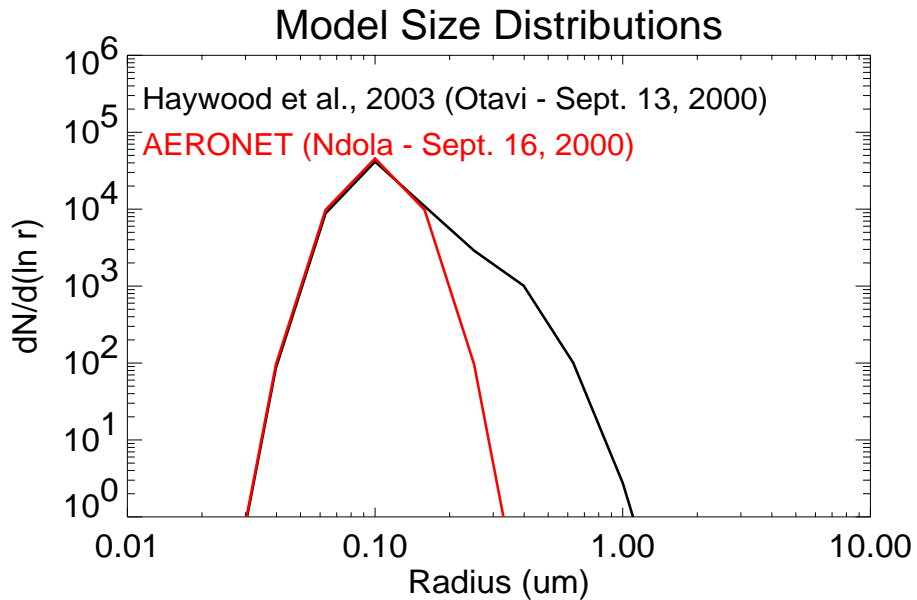


Figure 4. Initial aerosol size distributions used in Sensitivity Test #4. Aerosol size distributions were obtained from PCASP measurements (black line) and AERONET retrievals over Otavi, Namibia, Africa and Ndola, Zambia, Africa (red line), respectively.

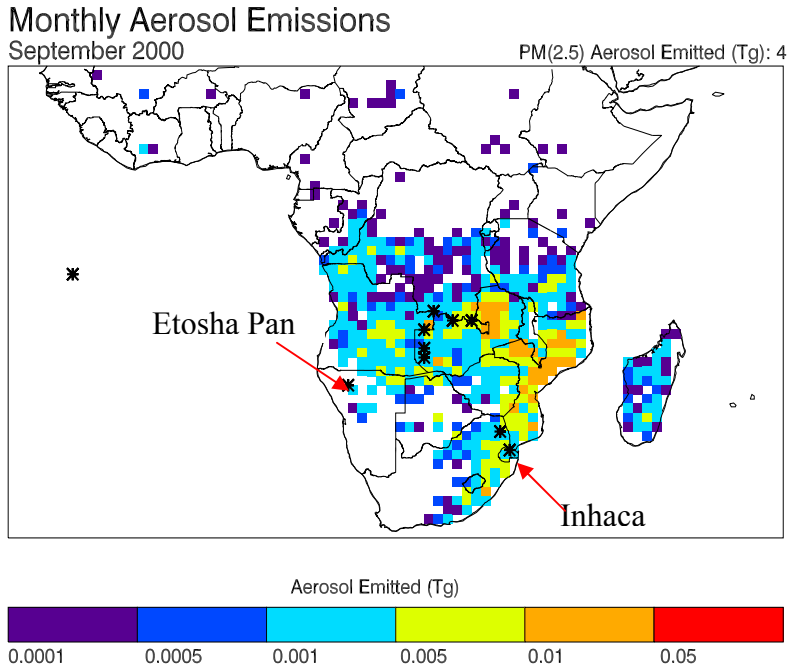


Figure 5. Monthly mean aerosol emissions over central and southern Africa during September 2000. Asterisks identify AERONET sites.

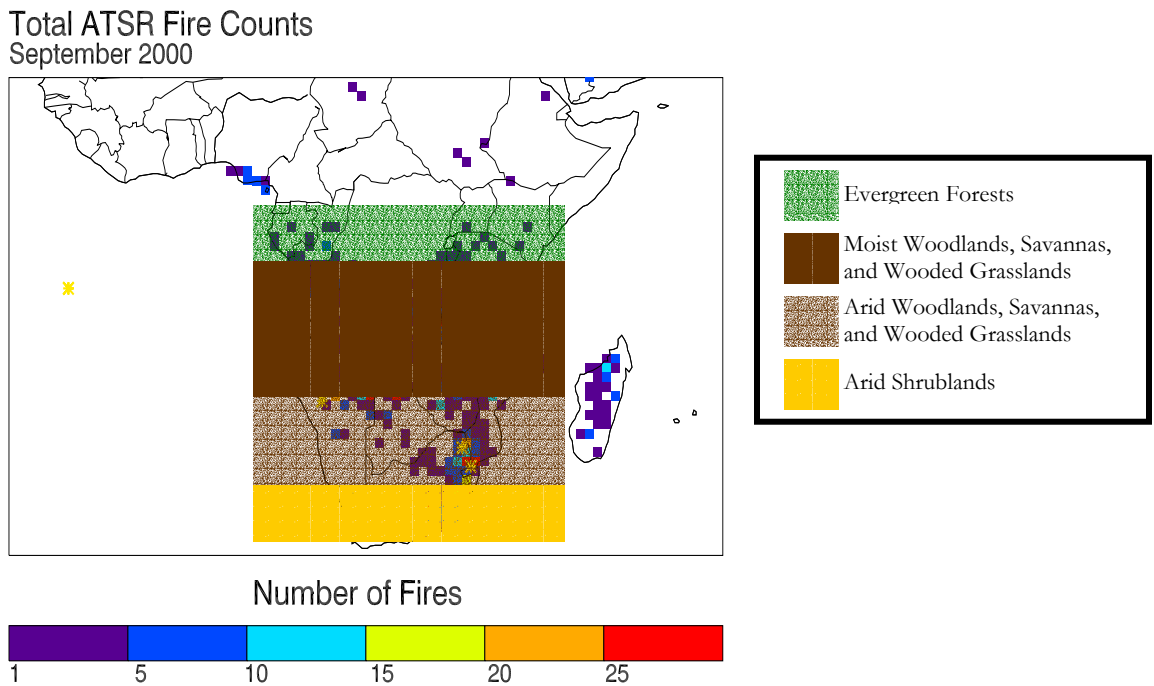


Figure 6. ATSR fire counts for the month of September 2000. Vegetation types for central and southern Africa are superimposed over the figure. Asterisks represent AERONET sites.

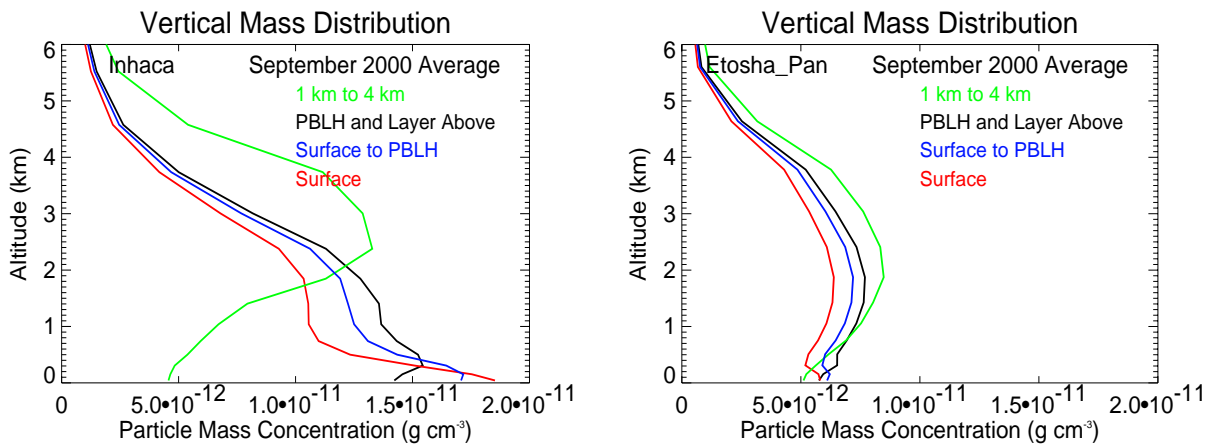


Figure 7. Modeled monthly mean vertical mass concentrations over Inhaca (Left) and Etosha Pan (Right) for September 2000 from Sensitivity Test #1.

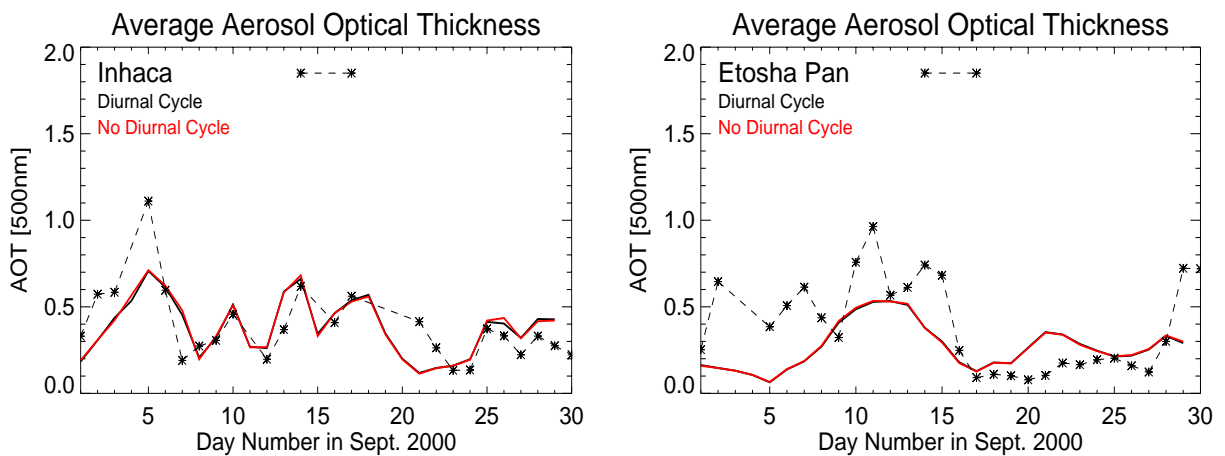


Figure 8. Modeled (solid line) and AERONET (asterisks connected by dashed line) daily mean AOT₅₀₀ for the month of September 2000 over Inhaca (Left) and Etosha Pan (Right) from Sensitivity Test #2.

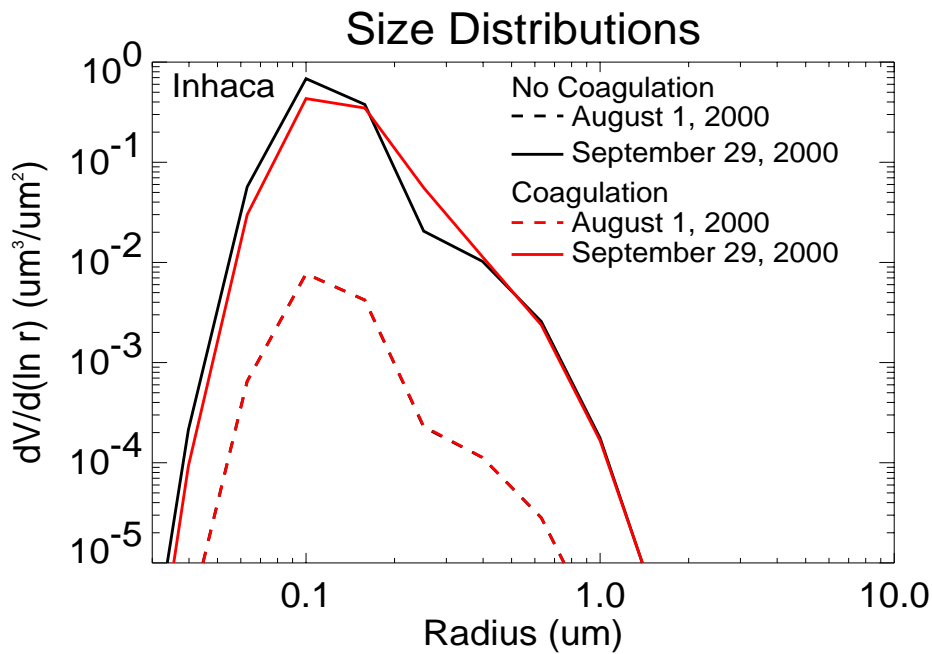


Figure 9. Daily mean volume size distributions over Inhaca on August 1, 2000 (dashed lines) and September 29, 2000 (solid lines) from Sensitivity Test #3.

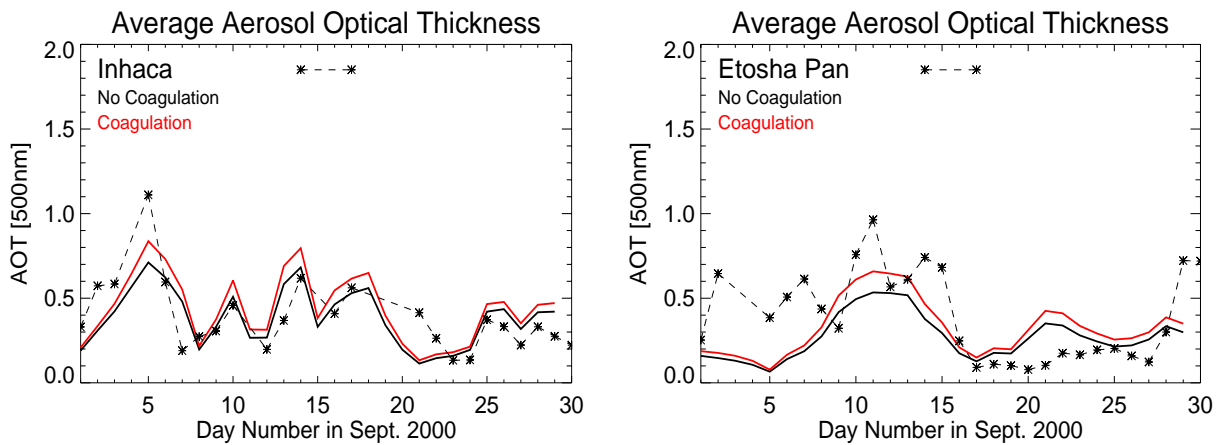


Figure 10. Modeled (solid lines) and AERONET (asterisks connected by dashed line) daily mean AOT_{500} for the month of September 2000 over Inhaca (Left) and Etosha Pan (Right) from Sensitivity Test #3.

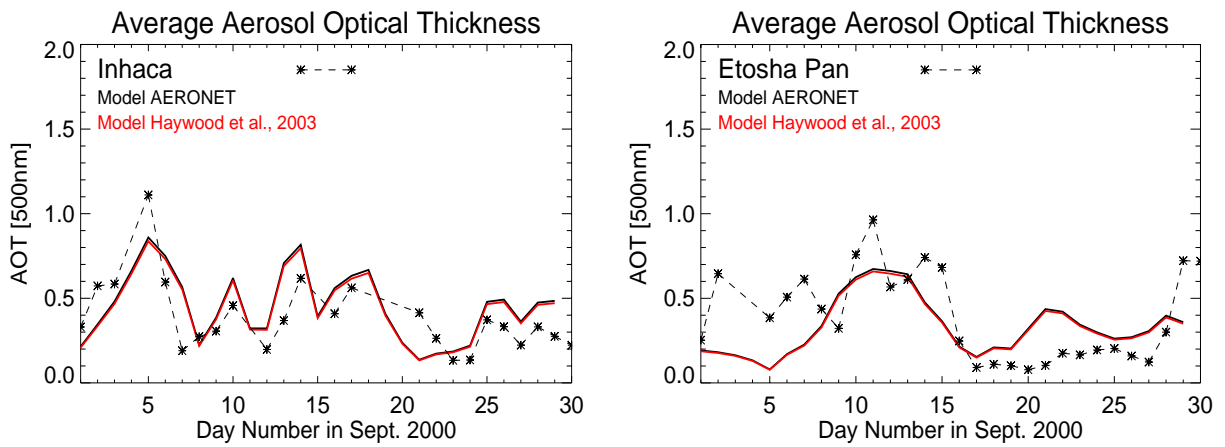


Figure 11. Modeled (solid lines) and AERONET (asterisks connected by dashed line) daily mean AOT_{500} for the month of September 2000 over Inhaca (Left) and Etosha Pan (Right) from Sensitivity Test #4.

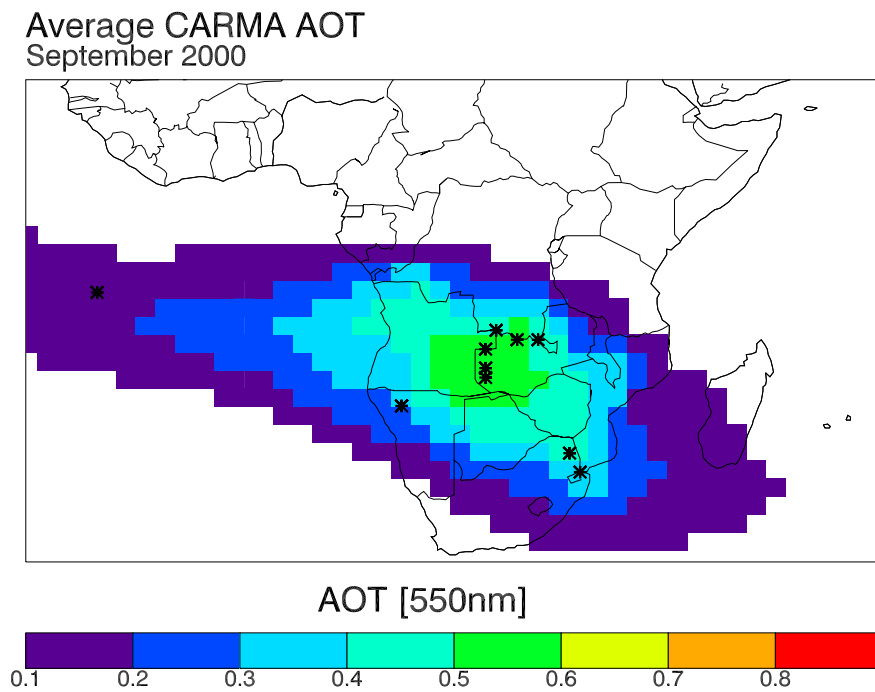


Figure 12. Modeled monthly mean AOT_{550} for the month of September 2000. The model was initialized using the conditions from Sensitivity Test #3. Asterisks identify AERONET sites.

Average EP-TOMS Aerosol Index
September 2000

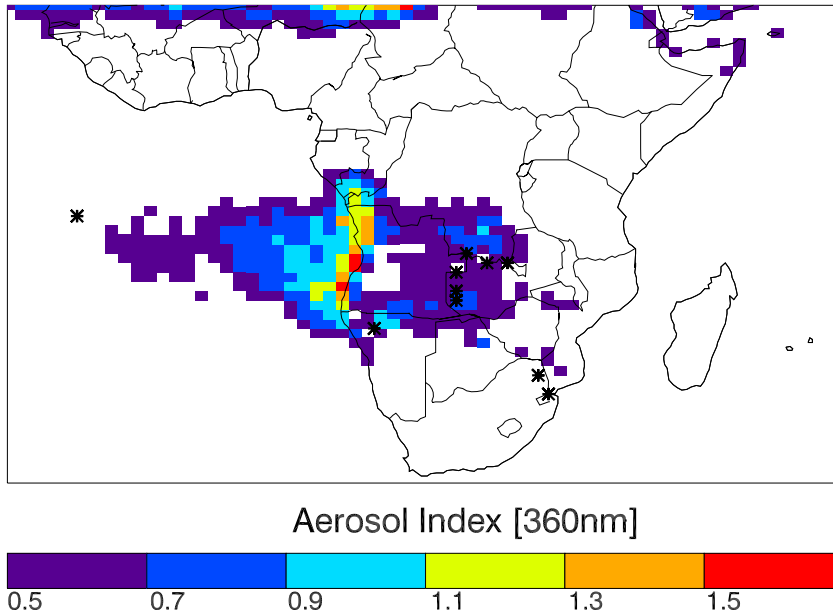


Figure 13. EP-TOMS monthly mean aerosol index at 360 nm. Asterisks identify AERONET locations.

Average MODIS AOT
September 2000

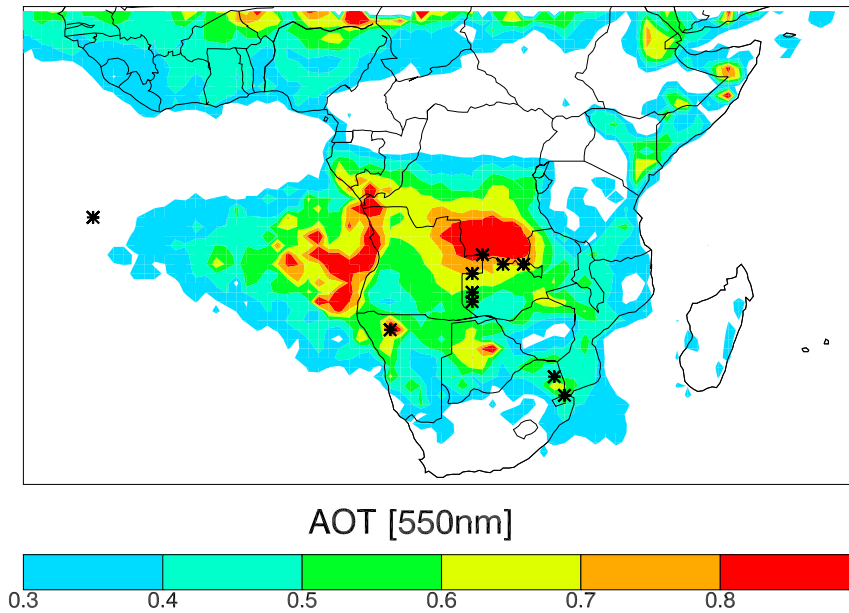


Figure 14. MODIS monthly mean AOT₅₅₀ for the September 2000. Asterisks identify AERONET sites.

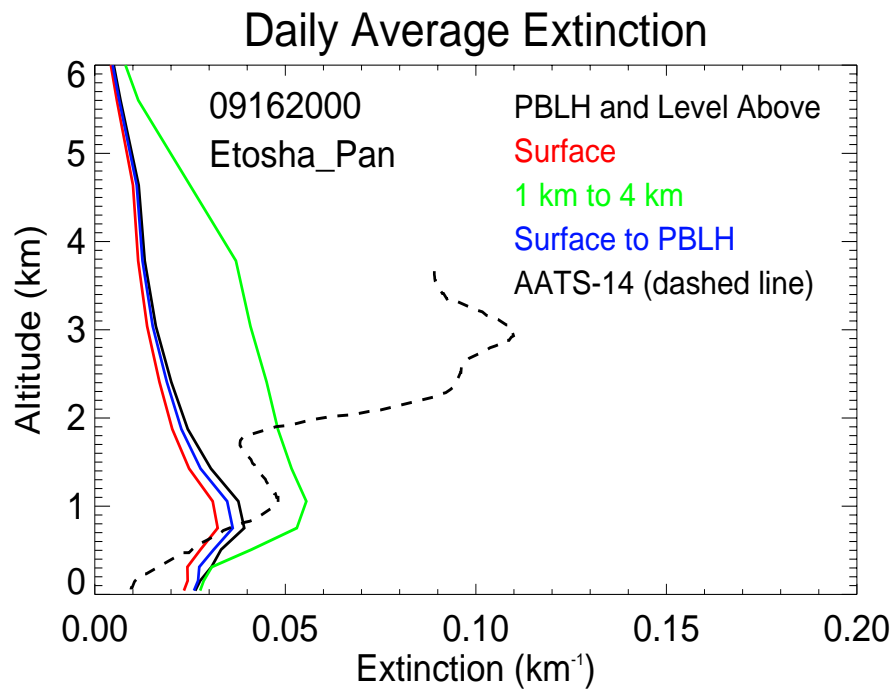


Figure 15. Modeled (solid lines) and AATS-14 (dashed line) daily mean extinction over Etosha Pan on September 16, 2000 from Sensitivity Test #1.

Etosha Pan Fires, 2000091612 (NMC 2.5x2.5 winds)
Backward Trajectories +/- 1° of Site

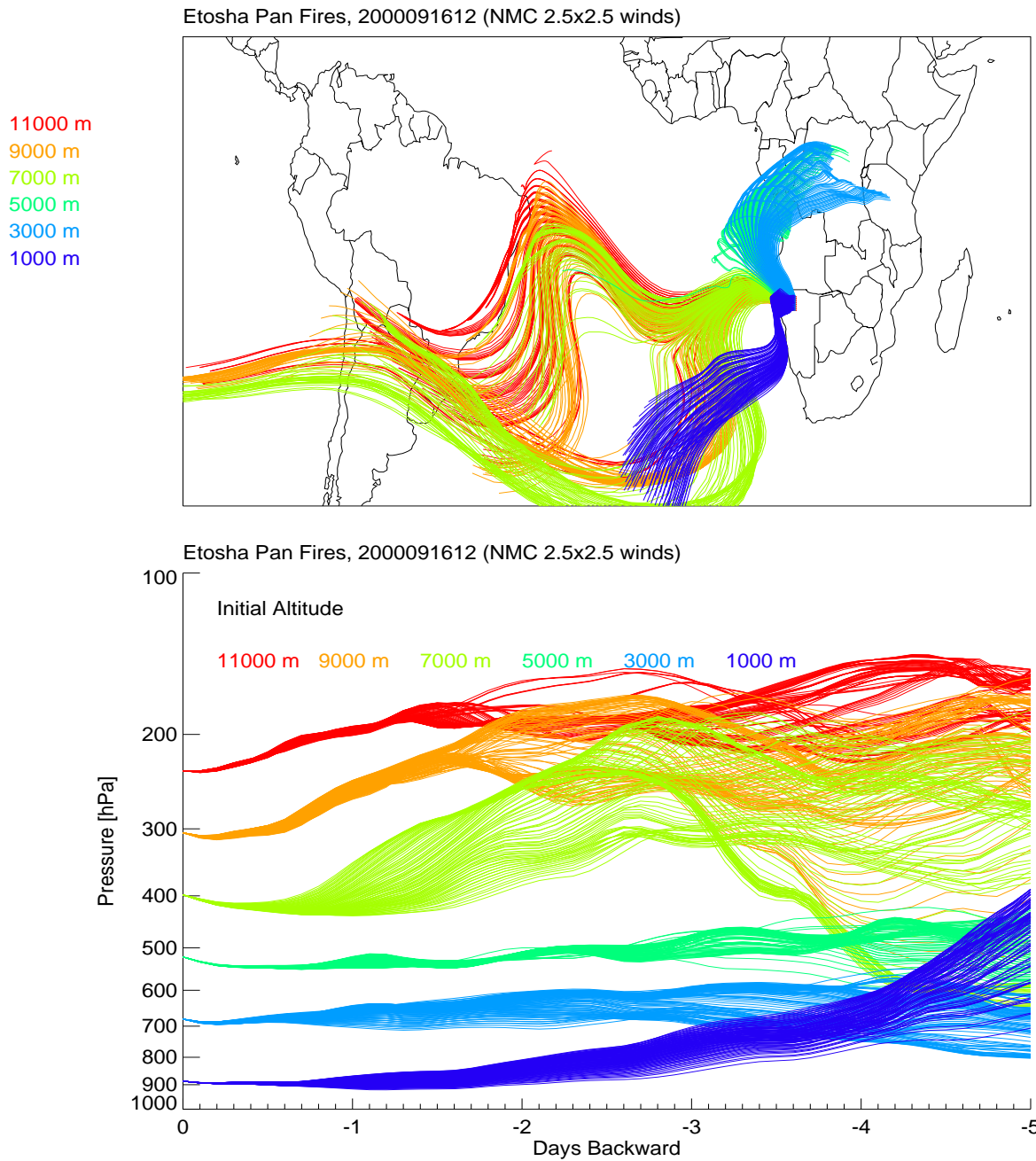


Figure 16. Back air mass trajectory starting at Etosha Pan on September 16, 2000 and going back 5 days at 1 km, 3 km, 5 km, 7 km, 9 km, and 11 km altitudes. The top panel is a top-down view of the air masses and the lower panel is a vertical view of the air masses.

Etosha Pan Fires, 2000091312 (NMC 2.5x2.5 winds)
Backward Trajectories +/- 1° of Site

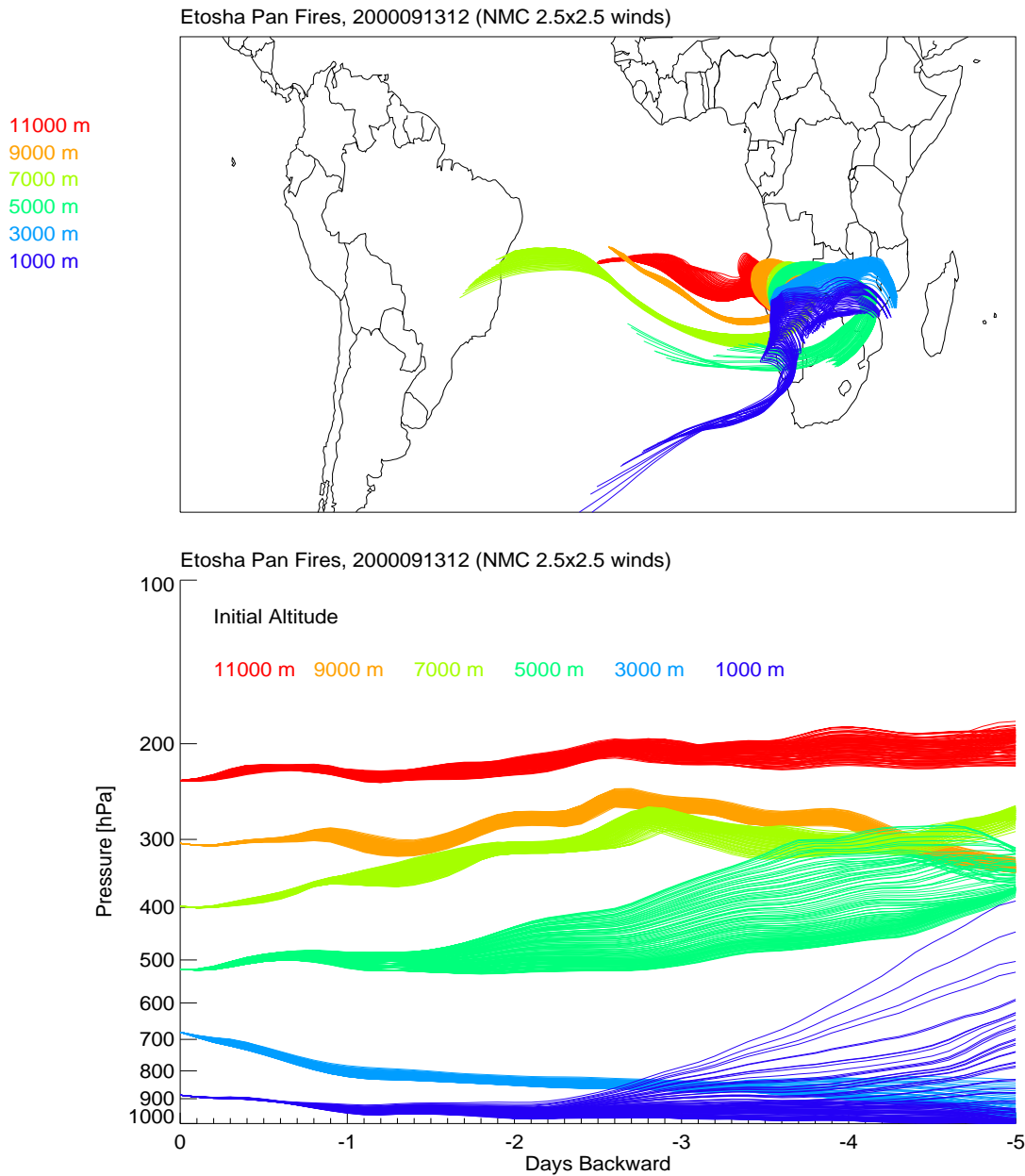


Figure 17. Back air mass trajectory starting at Etosha Pan on September 13, 2000 and going back 5 days at 1 km, 3 km, 5 km, 7 km, 9 km, and 11 km altitudes. The top panel is a top-down view of the air masses and the lower panel is a vertical view of the air masses.

Etosha Pan Fires, 2000092212 (NMC 2.5x2.5 winds)
Backward Trajectories +/- 1° of Site

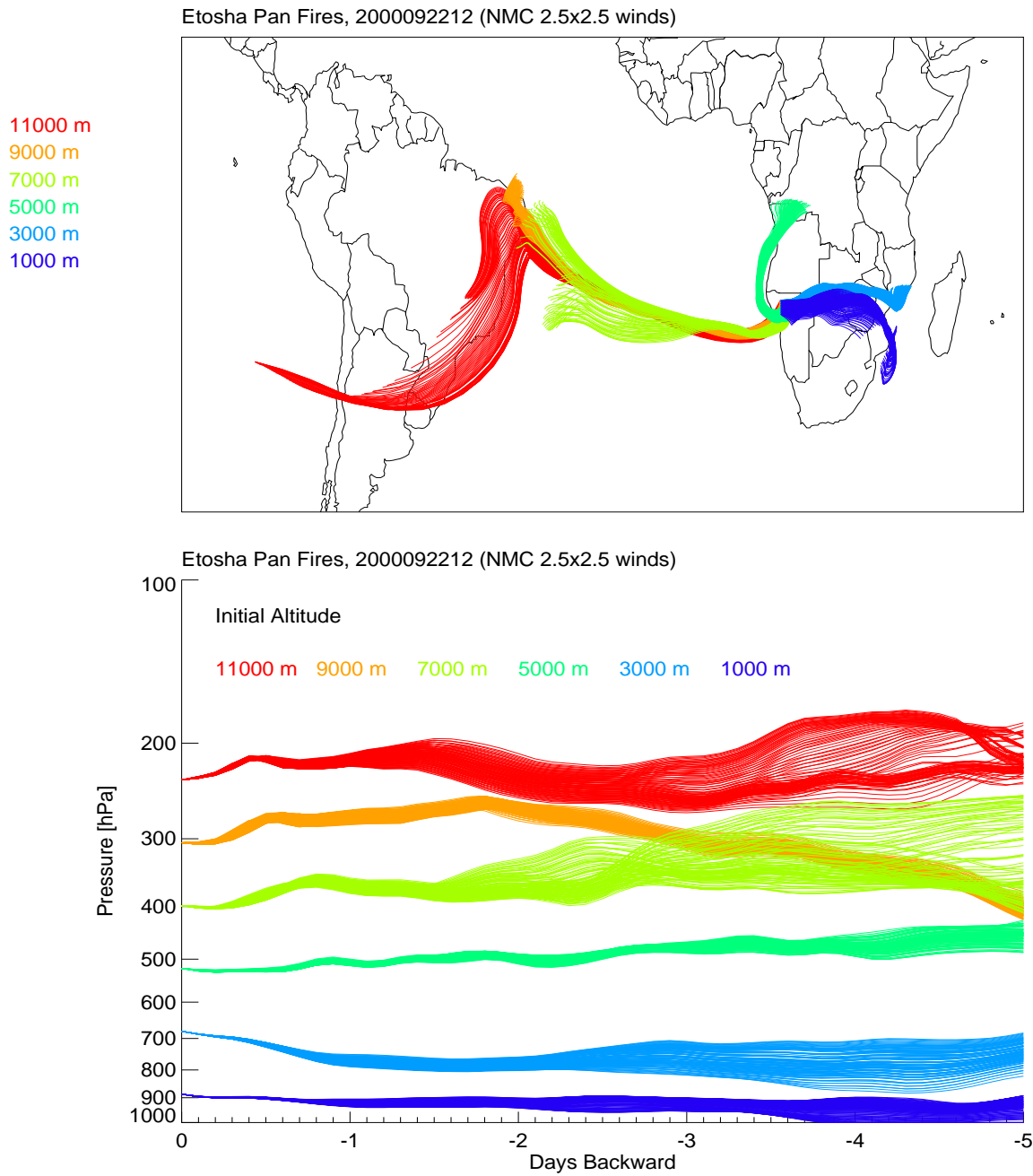


Figure 18. Back air mass trajectory starting at Etosha Pan on September 22, 2000 and going back 5 days at 1 km, 3 km, 5 km, 7 km, 9 km, and 11 km altitudes. The top panel is a top-down view of the air masses and the lower panel is a vertical view of the air masses.

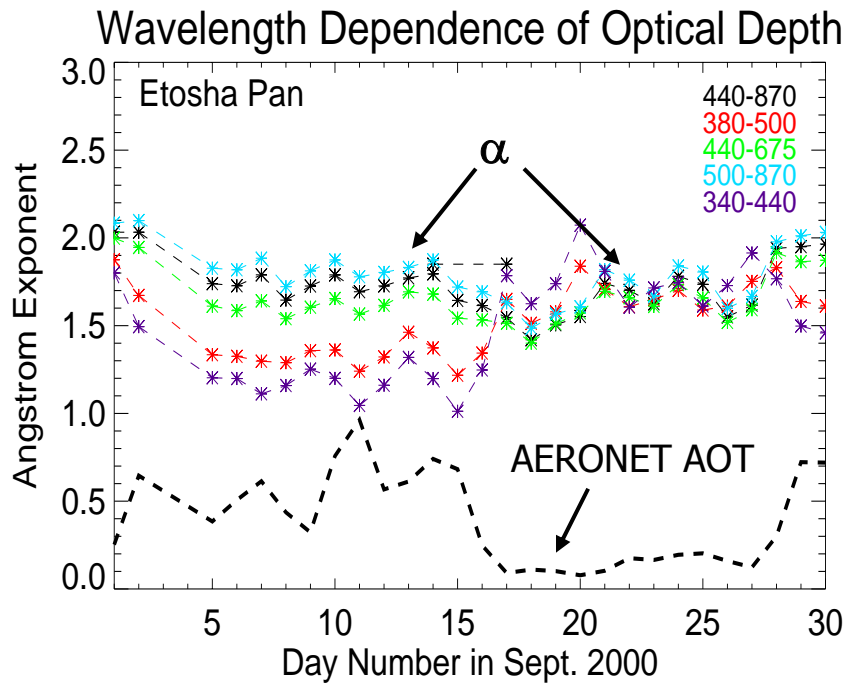


Figure 19. AERONET daily mean angstrom exponent pairs (asterisks connected by dashed line) and AOT₅₀₀ (black, dashed line) over Etosha Pan for the month of September 2000.

Table 1. Estimated Biomass Emissions (Tg yr⁻¹).

	Southern Africa	Savanna/Grassland
Total C	5168 (205-785 ^{6,7})	(480-3690 ^{1,2,3,4,5})
CO ₂	97 ⁹	(5096 ⁴)
CO	5 ⁹	(206 ⁴)
TPM	0.28-1.178 ¹⁰	(16.1 ⁴)
PM _{2.5}	0.3 ⁹	(26.2 ⁴)
OC	0.063-0.27 ¹⁰	(10.6 ⁴)
BC	0.007-0.017 ¹⁰	(1.5 ⁴)
NO _x	0.059-0.17 ¹⁰	(12.2 ⁴)
SO ₂	ND	(1.1 ⁴)

*Estimates in parentheses represent emissions not obtained during SAFARI 2000 campaign.

¹Seiler & Crutzen [1980]

²Hao et al. [1990]

³Crutzen & Andreae [1990]

⁴Andreae [1991]

⁵Hao and Liu [1994]

⁶Scholes et al.[1996]

⁷Barbosa et al.[1999]

⁸VanderWerf et al.[2003]

⁹Hely et al.[2003]

¹⁰Korontzi et al.[*in press*]

Table 2. Calculated ångström exponent pairs from Sensitivity Test #3 and AERONET over Etosha Pan on the 13 and 22 of September 2000.

Etosha Pan	$\alpha_{440/870}$	$\alpha_{380/500}$	$\alpha_{500/870}$
Sept. 13, 2000			
No Coagulation	2.35	1.92	2.52
Coagulation	1.89	1.42	2.03
AERONET	1.77	1.46	1.83
Sept. 22, 2000			
No Coagulation	2.35	1.92	2.52
Coagulation	1.90	1.42	2.05
AERONET	1.70	1.61	1.76